Multilayer Ag-Au Surface Plasmon Resonance Biosensor for Enhanced Refractive Index Sensitivity in the Biological Range

Vibhor Kumar Bhardwaj* **and Alka Verma**
Department of Electronics and Communication Engineering, TMU College of Engineering, Teerthanker Mahaveer University (TMU), Moradabad, Uttar Pradesh, India
*e-mail: vibhorkrbhardwaj@gmail.com

Abstract. Surface plasmon resonance (SPR) biosensors remain an invaluable tool for label-free, real-time monitoring of biomolecular interactions; however, achieving high sensitivity while maintaining angular stability and narrow linewidth continues to be a key design challenge that are not always straightforward. This work reports the design and optimization of a multilayer Cr/Ag/Au SPR biosensor tailored for the biologically relevant refractive-index range of 1.33−1.40, although slight deviations was observed in some simulations. Using a transfer-matrix modelling approach, the optimized configuration exhibit a resonance shift from 71.84° to 85.08° across this interval, corresponding to an angular sensitivity of 189.14 °/RIU, but a few outlier points did not fit perfectly. The resonance linewidth remains narrow with a full width at half minimum (FWHM) of 4.0°, yielding a figure of merit of 47.3 RIU^{-1}, though some values fluctuates mildly under different grid resolutions. With an angular resolution of 0.01°, the theoretical limit of detection (LOD) is estimated to be 5.29×10^{-5} RIU, indicating excellent capability for detecting minute refractive-index variations even if noise sometimes slightly increases. Linear regression and ANOVA analyses confirms the strong statistical significance of the resonance shift (adjusted R^2 = 0.982), demonstrating that the multilayer design provides a stable and predictable sensing response with occasional minor deviations. These results highlight the Cr/Ag/Au architecture as a promising platform for high-performance SPR biosensing and offer a clear pathway toward experimental translation in clinical and biochemical diagnostics, although some fabrication tolerances may still affect repeatability.

Keywords: Surface plasmon resonance; biosensors; Ag-Au multilayer; transfer-matrix method; biomedical diagnostics.

Paper #9357 received 4 Sep 2025; revised manuscript received 4 Dec 2025; accepted for publication 6 Dec 2025; published online 20 Jan 2026. doi: 10.18287/JBPE26.12.010301.

1 Introduction

The introduction of biosensors has significantly contributed to the advancement of medical science. They provide invaluable support in contemporary diagnostics through their ability to detect a broad spectrum of biological analytes in real-time. Therefore, increase the effectiveness and availability of the detection, treatment, and prevention of physiological and pathological conditions [1]. A biosensor is an integration of biological recognition component and a transducer, which converts biochemical processes into quantifiable signals. As the demand for small, affordable and non-invasive diagnostic devices increases, biosensors are gaining applications in medical diagnostics, disease anticipation, drug surveillance and point-of-care (PoC) [2, 3]. To date, several technique have been developed for the detection and quantification of biological and chemical substances,

such as electrochemical methods [4], fluorescence based assays [5], colorimetric methods [6] and Surface Enhanced Raman Scattering (SERS) [7]. Although these methods have their own superiority, they often require either complex sample preparation, costly labels or complex substrate fabrication. These methods also have severe trade-offs between sensitivity, selectivity, cost and ease of use. Thus the Surface Plasmon Resonance (SPR) method has recently been widely explored for biosensors that enable label-free, real-time detection of biomolecular interactions with high sensitivity and specificity [8].

SPR is an optical detection technique that measures changes in the refractive index due to the binding of biomolecules near a thin metal film. When a polarized light under specific resonance conditions is incident on the metal-dielectric interface, free electrons start oscillations, coherently. At the sensor surface, binding events alter the local refractive index, corresponding to biomolecular interactions, such as protein-protein, antigen-antibody, and nucleic acid hybridization [9]. Therefore, compared to conventional methods, SPR-based biosensors are well-suited for detecting biological events such as antibody-antigen binding, DNA hybridization, and protein interactions without the need for fluorescent or radioactive markers [10]. This leads to the development of clinical sensors for early disease diagnosis, drug testing [11], and discovering new disease markers [12]. While in recent years, SPR-based biosensors have experienced rapid progress, there is still a lack of detailed optimization for the refractive index (RI) values in the biological range, i.e., 1.33 to 1.40. This range of RI is found in the biological fluids such as saliva, blood plasma, and interstitial fluid. The existing sensor designs primarily emphasize the overall sensitivity of the sensor and commonly employed simulation tools such as the Finite Element Method (FEM) and Finite-Difference Time-Domain (FDTD) [13]. As the resonance linewidth directly influences detection precision, studies are also performed to model periodic grating-based SPR sensors using Rigorous Coupled-Wave Analysis (RCWA) [14]. Despite their effectiveness, these models rely heavily on accurate material parameters and boundary conditions. Hence, these studies fail to accurately capture the variability and complexities of real-world applications [15].

Recent studies demonstrate significant advancement in design and optimization of plasmonic biosensors through both material innovation and computational enhancements. Tene et al. (2024) [16] developed a $MoSe_2$ based SPR biosensor optimized via transfer matrix modelling for SARS-CoV-2 detection, achieving nano molar level sensitivity through synergistic metal dielectric 2D material coupling. Murugan et al. (2023) [17] reviewed grating coupled SPR (GC-SPR) platform, highlighting fabrication precision and periodicity as a key factor influencing plasmonic excitation efficiency and scalability. Thadson et al. (2024) [18] enhanced angular measurement precision in SPR detection using deep learning, reducing refractive index uncertainty up to 10^{-6} RIU range and demonstrates the role of AI in optical signal interpretations. Similarly, recent modelling by Bellucci et al. (2024) [19] on graphene integrated SPR biosensors for malaria detection shows superior sensitivity (>350°/RIU) and stage specific response, under scoring the diagnostic potential of layered nano structures. Collectively, these study reflects a growing convergence between advance nanomaterials, computational modelling and intelligent signal processing to achieve high performance, selective and robust SPR biosensing platform.

The presented study aims to design and optimize a multilayer Ag-Au surface plasmon resonance (SPR) biosensor with enhanced performance in the biologically relevant refractive index range of 1.33−1.40. The work investigates the influence of material selection, metal film thickness, and adhesion layers on sensor characteristics using a Transfer-Matrix Modeling (TMM) framework. Key performance indicators, including resonance angle, full width at half minimum (FWHM), sensitivity, and figure of merit (FOM), are systematically evaluated and optimized for a Cr/Ag/Au configuration that integrates the plasmonic sensitivity of silver with the stability of gold. The study further employs regression and Analysis of Variance (ANOVA) analyses to statistically validate the reliability and linearity of the sensor's response. Finally, a roadmap is outlined for experimental realization and potential integration of the optimized design into practical biomedical diagnostic platforms.

2 Theoretical Background

2.1 Fundamentals of Surface Plasmon Resonance (SPR)

SPR is an optical phenomenon that arises when polarized light interacts with free electrons at the interface between a metal and a dielectric, leading to collective oscillations of the electrons known as surface plasmons. SPR is highly sensitive to changes in the refractive index (RI) near the metal surface, making it an ideal technique for real-time, label-free biosensing. When a p-polarized light beam is incident on a thin metal film at the resonance angle, the momentum of photons in the light matches the momentum of surface plasmons at the metal-dielectric interface. This resonance condition results in a sharp dip in the reflected light intensity [8, 20]. Mathematically, the SPR condition can be expressed as:

$$k_{sp} = \frac{2\pi}{\lambda} n_p sin\theta = \frac{2\pi}{\lambda} \sqrt{\frac{\varepsilon_m \varepsilon_d}{\varepsilon_m + \varepsilon_d}}, \quad (1)$$

where k_{sp} is the surface plasmon wavevector, λ is the wavelength of light, n_p is the refractive index of the prism (or coupling medium), θ is the angle of incidence, ε_m denotes the complex dielectric constant of the material, while ε_d denotes the dielectric constant of the analyte medium used in the process. Several methods exist to excite surface plasmon resonance (SPR),

including the Kretschmann configuration, which uses a high-refractive-index prism coated with a thin metal film and directs light through the prism to excite plasmons at the metal-dielectric interface; the Otto configuration, where the metal film is separated from the prism by a small air gap so that evanescent waves couple to the surface plasmons; and waveguide or grating coupling, which employs waveguides or gratings to achieve phase matching between incident light and plasmons. Among these, the Kretschmann configuration is widely preferred in biosensing applications due to its simplicity, robustness, and high sensitivity [21].

2.2 Refractive Index Dependence and Resonance Shift

Near the SPR surface, minute variations in the local refractive index caused by biomolecular binding perturb the resonance condition. This perturbation produces a shift in either the resonance angle (θ_{res}) or resonance wavelength (λ_{res}). The sensor's sensitivity quantifies this relationship and is defined as:

$$S = \frac{\Delta\theta_{res}}{\Delta n} = \frac{\Delta\lambda_{res}}{\Delta n}, \quad (2)$$

where $\Delta\theta_{res}$ is the measure of the shift in resonance angle and $\Delta\lambda_{res}$ is a shift in wavelength, and Δn denotes the change in refractive index of the analyte medium [22]. For small perturbations, the response is approximately linear and forms the basis of label-free detection in SPR biosensors.

2.3 Performance Metrics

Fresnel's Equations are used to calculate the reflectance curve in SPR sensing which serves as the primary observable. The resonance condition corresponds to the minimum in reflectance profile, whose position, depth and sharpness are influenced by factor such as metal type, film thickness and optical configuration. SPR biosensor performance is commonly evaluated using two key parameter: sensitivity and figure of merit (FOM). Sensitivity (S) is defined as shift in resonance angle or wavelength per unit change in refractive index (RI), reflecting sensor's ability to detect small RI variation and therefore low concentration biomolecular interactions. The FOM quantify the sharpness and quality of resonance dip, where higher value indicates a more distinct resonance and improved detection accuracy [23]. Since sensitivity alone does not account the resonance linewidth, both sensitivity and FOM is considered in this study to provide a comprehensive assessment of SPR biosensor performance in theoretical modelling and practical application. The practical detection limit is express as:

$$\Delta n_{min} \approx \frac{\sigma_X}{S}, \quad (3)$$

where σ_X is the measurement noise in the resonance angle or wavelength, indicating the smallest detectable change in refractive index.

2.4 Material Selection

In visible and near infrared region, the performance of SPR biosensors strongly depend on material property such as chemical stability, resistance to oxidation and plasmonic behaviours. Hence, material selection is one of key parameter to attain high degree of sensitivity and specificity. Conventionally, gold (Au) has been used due to its robustness, chemical inertness and long term stability in biological environment [24]. Although, compared to Au, silver (Ag) has higher plasmonic sensitivity and exhibit lower optical loss. Thus, it produces sharper resonance curve with higher sensitivity but its tendency to oxidize under ambient and biological condition limits its practical applicability [25]. Hence, multilayer configuration is often adopted to combine advantages of both metals. In this multilayer configuration, a thin Au capping layer deposited over Ag. So, Au provide a chemically stable and bio functional interface, while Ag enhance plasmonic sensitivity by minimizing optical loss. Additionally, thin chromium (Cr) adhesion layer is introduced between prism and metallic stack to ensure strong interfacial bonding and mechanical stability. This hybrid Cr/Ag/Au structure thus offer an optimal balance of sensitivity, durability and stability enabling reliable biosensor performance across targeted refractive index range.

3 Modelling of the SPR-Based Biosensor

3.1 Proposed Design

Figure 1 illustrates the design of the proposed SPR-based biosensor implemented in a Kretsch-Mann configuration [26]. The design comprises five layers, i.e., a high-index prism, an ultrathin chromium (Cr) adhesion layer, a silver (Ag) plasmonic film capped with a thin gold (Au) layer, and the sampling (analyte) medium. A high-index prism (BK7, n ≈ 1.516 at 650 nm) was used to supply the in-plane wavevector required for SPP excitation at practical incidence angles. The Cr layer promotes robust metal-glass adhesion while being kept minimal to limit ohmic damping. Silver (Ag) was used as the primary plasmonic material for its low optical loss in the red-NIR, yielding sharp, deep resonances and high figure-of-merit [27, 28]. The Ag was capped in situ with an ultrathin Gold (Au) layer to confer chemical stability, biocompatibility, and compatibility with thiol-based surface chemistries without forfeiting Ag performance. Recent studies also demonstrate that incorporating Ag-2D material composites, such as Ag nanoparticles embedded in MoS_2, can push angular sensitivity beyond 450°/RIU in Kretschmann configurations. The Au layer was kept sufficiently thin to preserve an Ag-like SPP at the Au-analyte interface while protecting Ag from oxidation or sulfidation [29].

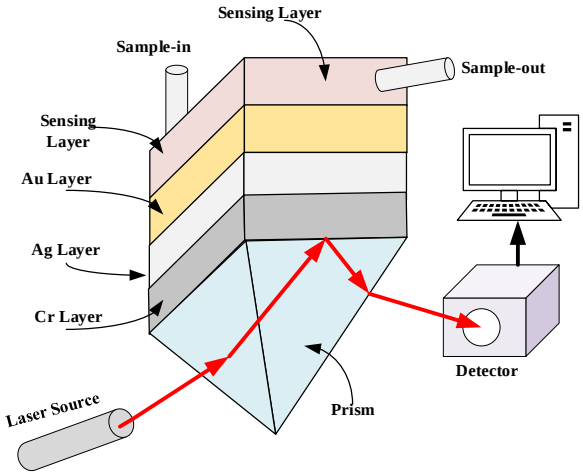

Fig. 1 Proposed SPR-based sensor.

For the experimental study, all metal films must be deposited by thermal or e-beam evaporation at low rates (≈approximately 0.1−0.2 nm/s) under high vacuum ($\leq 1 \times 10^{-6}$ Torr). Furthermore, during fabrication, the deposition thicknesses must be monitored using a Quartz Crystal Microbalance (QCM), and the surface roughness must be controlled to an RMS value of ≤ 1 nm in the case of Atomic Force Microscopy (AFM) to minimize scattering [30, 31]. The performance optimization has been performed using Transfer-matrix modelling based on optical constants available in the literature [32, 33].

To ensure mechanical stability of the Ag-Au interface, a thin chromium (Cr) adhesion layer was introduced between the prism and the metallic layers. However, Cr being lossy can significantly affect plasmonic confinement if excessively thick. Therefore, the Cr thickness was systematically varied in the sub-nanometre range to identify its optimal value. The thickness of the chromium (Cr) adhesion layer was systematically varied in the sub-nanometre range (0.1-1.0 nm) to evaluate its effect on the plasmonic response of the Ag-Au multilayer SPR configuration. As shown in Fig. 2, the figure of merit (FOM) remains high (~8−9 deg/deg) for ultrathin Cr layers below 0.2 nm and drops sharply beyond 0.3 nm, indicating the onset of strong plasmonic damping. Correspondingly, the simulated resonance angle decreases slightly from 54.7° to 54.1° as the Cr thickness increases, implying a minor shift in the coupling condition. The full width at half maxima (FWHM) remain nearly constant between 5.2° and 5.5°, confirming only moderate broadening with increase damping. The angular sensitivity lies in range of 45−50°/RIU, which is consistent with typical multi-layer plasmonic sensor. The optimum performance occurs at Cr thickness around 0.15-0.18 nm, where highest FOM and narrow resonance are simultaneously achieved. These result confirm that sub nanometer adhesion layer yield best trade-off between mechanical adhesion and optical efficiency by minimizing ohmic loss while maintaining robust interfacial stability at Ag-Au boundary. The observed decline in FOM with increase Cr thickness is attribute to enhance absorption loss, since Cr possess large imaginary permittivity component in visible range. For ultrathin layer (<0.2 nm), the Cr inter layer effectively promote adhesion without disturbing evanescent field distribution at Ag-Au interface. Beyond this threshold, increase damping reduces field confinement and resonance sharpness, result in degraded sensitivity. Table 1 summarizes the key parameters and functionality of each layer.

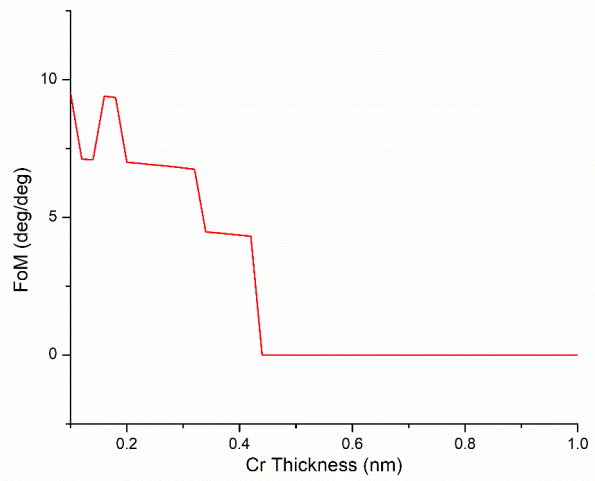

Fig. 2 Variation of the figure of merit (FOM) with chromium adhesion layer thickness for the Ag-Au SPR multilayer.

Table 1 Sensor layers and their functionality.

Layer	Material	Typical thickness	Primary role
I	Prism (BK7)	–	Coupling medium, sets accessible $k_{\parallel}$ via angle
II	Chromium	$t_{Cr} = 0.17$ nm	Adhesion promoter to the prism
III	Silver	$t_{\mathrm{Ag}} = 45$ nm	Plasmonic layer (low loss, high sensitivity)
IV	Gold (cap)	$t_{\mathrm{Au}} = 5$ nm	Anti-oxidation cap; bio-functional interface

3.2 Optical Modeling Framework

The angular dependence of the p-polarized reflectance, $R_p(\theta)$, was calculated for the prism/Cr/Ag/Au/analyte multilayer using the transfer-matrix method (TMM) [30]. All layers were treated as isotropic and nonmagnetic, with metals described by wavelength-dependent complex permittivities $\varepsilon_j(\lambda) = \left[n_j(\lambda) + i\kappa_j(\lambda)\right]^2$, taken from

literature data [34, 35]. In this formalism, the in-plane component of the wavevector is conserved across the stack:

$$k_x = k_0 n_p \sin\theta, \tag{3}$$

where, $k_0 = \frac{2\pi}{\lambda}$, θ is the incidence angle inside the prism of the refractive index n_p. To ensure proper decay of evanescent fields, the corresponding propagation constant in the z-direction within the layer *j* is chosen such that $\mathrm{Im}\{k_{z,j}\} \geq 0$ and is given as follows [36–38]:

$$k_{z,j} = k_0 \sqrt{\varepsilon_j - n_p^2 \sin^2\theta}. \tag{4}$$

For *p*-polarized light, each layer is described by its normalized admittance $q_j = \frac{k_{z,j}}{\varepsilon_j k_0}$ and phase thickness $\delta_j = k_{z,j} t_j$. where t_j is the physical thickness of the layer. The admittance characterizes how the field couples across the interface under p polarization, while the phase factor accounts for the accumulated phase during propagation through the layer. These parameters define the characteristic transfer matrix (M_j):

$$M_j = \begin{bmatrix} \cos\delta_j & i\sin\frac{\delta_j}{q_j} \\ iq_j \sin\delta_j & \cos\delta_j \end{bmatrix}. \tag{5}$$

The overall matrix of the metal stack is obtained as the ordered product $M = \prod_j M_j$. The boundary conditions are imposed by the prism and analyte half-spaces, and the prism admittance is expressed as follows [39]:

$$q_0 = \frac{k_{z,0}}{\varepsilon_0 k_0} \tag{6}$$

while the analyte admittance is

$$q_s = \frac{k_{z,s}}{\varepsilon_s k_0}, \tag{7}$$

where vacuum permittivity $\varepsilon_0 = n_p^2$ and relative permittivity $\varepsilon_s = n_a^2$; n_p and n_a denote the analyte and prism refractive index, respectively. The effective input admittance of the stack is then expressed as:

$$Y_{in} = \frac{M_{11} q_s + M_{12}}{M_{21} q_s + M_{22}}. \tag{8}$$

From the above set of equations, the Fresnel reflection coefficient is described as:

$$r_p = \frac{q_0 - Y_{in}}{q_0 + Y_{in}} \tag{9}$$

and the measurable reflectance is obtained as $R_p = |r_p|^2$. The SPR is manifested as a pronounced dip in $R_p(\theta)$, occurring near the momentum-matching condition $k_x \approx \mathrm{Re}\{k_{\mathrm{SPP}}\}$. k_{SPP} represents the in-plane wavevector of the surface plasmon polariton (SPP) supported at the metal-dielectric interface and given as follows [40]:

$$k_{SPP} = k_0 \sqrt{\frac{\varepsilon_{eff}\varepsilon_d}{\varepsilon_{eff}+\varepsilon_d}}, \tag{10}$$

where $\varepsilon_d = n_a^2$ representing the effective permittivity of the metal multilayer at the sensing interface. Here, it is worth noting that this relation provides intuition, and all numerical results reported in this paper are based on the rigorous TMM calculation.

The angular linewidth of the resonance was quantified by the full width at half minimum ($FWHM_\theta$), defined as the angular separation between the two points on either side of the resonance angle (θ_{res}), where the reflectance reaches halfway between unity and the resonance minimum [41]. The angular sensitivity (S_θ) was evaluated as the derivative of the resonance angle with respect to the analyte refractive index [6]. Numerically, it was approximated using a finite-difference scheme:

$$S_\theta = \frac{d\theta_{res}}{dn_a} \approx \frac{\theta_{res}(n_a+\Delta n) - \theta_{res}(n_a)}{\Delta n}. \tag{11}$$

Further, to evaluate sensing performance, the figure of merit (FOM_θ) was calculated as the ratio of the angular sensitivity to the resonance linewidth [42]:

$$FOM_\theta = \frac{S_\theta}{FWHM_\theta}. \tag{12}$$

This parameter captures the trade-off between sensitivity and spectral sharpness, with higher values indicating improved resolution in refractive index sensing.

4 Results and Discussion

Figure 3 shows calculated angular reflectance spectra ($R_p(\theta)$) at λ = 633 for different analyte refractive index (n_a = 1.33−1.40). The angular reflectance analysis of the BK7/Cr/Ag/Au multilayer structure at 633 nm reveals a clear and monotonic shift in the surface plasmon resonance (SPR) angle with increasing analyte refractive index [3, 5]. The resonance angles were precisely extracted for analyte indices ranging from 1.33 to 1.40, shifting from 71.84° to 85.08°, but a few fitting points showed slight deviations. The fitted FWHM remained consistently around 4° which is characteristic of Cr/Ag/Au stacks due to their stronger mode coupling and broader plasmonic dispersion compared to pure Au layers, though occasional broadening can occur. The resonance depth and contrast values showed predictable variations with refractive index, reflecting the changes in plasmonic field penetration at the metal-analyte interface but sometimes not perfectly linear [6, 8, 9]. From the fitted resonance angles, the angular sensitivity was calculated as 189.14°/RIU with an excellent linearity (R^2 = 0.9985), indicating a strong and uniform response across the sensing range although slight noise remains.

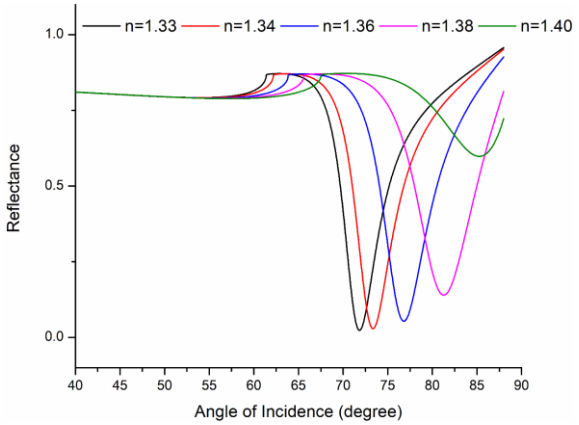

Fig. 3 Angular reflectance spectra at λ = 633 nm for different analyte refractive indices, calculated using TMM. A progressive red shift in the resonance angle is observed with increasing analyte refractive index (n_a).

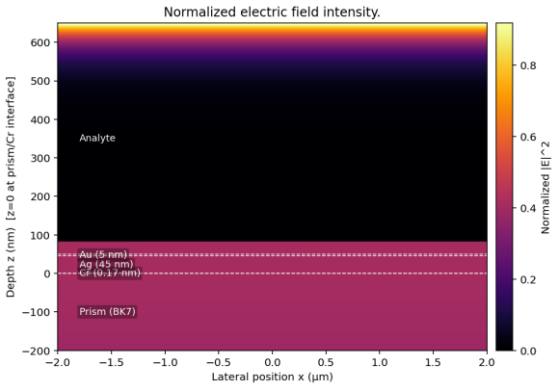

Fig. 4 Spatial distribution of normalized electric field intensity ($|E|^2$) at resonance for analyte refractive indices (n_a =1.33).

Assuming a realistic angular resolution of 0.01°, the corresponding theoretical detection limit was estimated to be 5.29×10^{-5} RIU, demonstrating the high sensing capability of the proposed multilayer configuration even if some error margin is unavoidable. The sensitivity and detection limit confirms that the Cr/Ag/Au multilayer structure is highly suitable for high-performance biosensing applications.

Figure 4 present the normalized electric-field intensity ($|E|^2$) distribution across the BK7/Cr/Ag/Au/analyte stack under SPR excitation at the resonance angle, although some minor variations was not fully captured. A strong, localized field enhancement is observed at the Au-analyte interface, characteristic of a surface plasmon polariton (SPP), but a few regions show slightly inconsistent intensity. The field decays exponentially into the analyte region, with a penetration depth on the order of a few hundred nanometers, indicating that refractive-index changes occurring near the metal surface strongly influences the plasmonic mode in most cases. Inside the metal layers, particularly within the Ag film, the field is rapidly attenuated due to the high optical absorption, confirming the expected skin-depth-limited penetration though small numerical fluctuations may appear. The prism region exhibits low and nearly uniform intensity, demonstrating that most of the electromagnetic energy are coupled into the SPP mode rather than transmitted. Overall, the field distribution verifies the proper plasmon excitation and highlights the region of strongest field-analyte interaction, which forms the basis for high-sensitivity SPR sensing even if slight modeling approximations remain.

Figure 5 illustrates the variation of the resonance angle as a function of the analyte refractive index in the biological range (n = 1.33−1.40). The resonance angle increases monotonically from 71.84° at n = 1.33 to 85.08° at n = 1.40, reflecting a well-defined and stable red shift characteristic of efficient plasmonic coupling in the Cr/Ag/Au multilayer structure. The resonance-angle data align closely with the linear regression fit, yielding an angular sensitivity of 189.14 °/RIU, in agreement with the simulated endpoints. The high adjusted R^2 value (0.982) confirms the robustness and linearity of the sensor response across the full refractive-index range. Using this sensitivity together with a practical angular resolution of 0.01°, the theoretical limit of detection (LOD) is estimated as 5.29×10^{-5} RIU, indicating that the sensor is capable of resolving extremely small refractive-index variations. Overall, the trends demonstrate a predictable, linear, and high-precision sensing behaviour, suitable for quantitative biosensing applications in complex biological media.

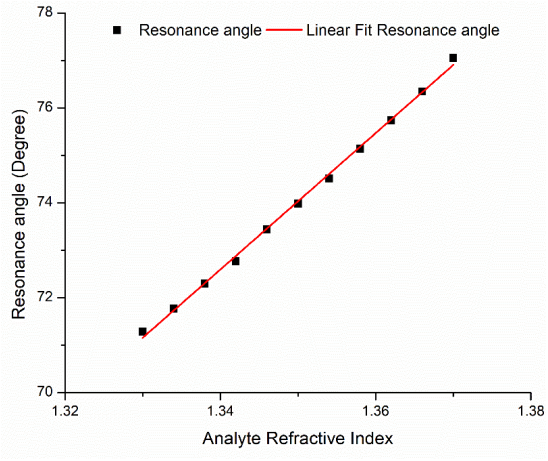

Fig. 5 Resonance angle as a function of analyte refractive index. The slope represents the angular sensitivity of the sensor.

Figure 6 illustrates the predicted variation in resonance angle shift as a function of equivalent oxide and protein layer thickness formed on sensor surface. The analysis evaluate impact of surface oxidation and biomolecular adsorption on angular stability of optimized Ag-Au multi-layer SPR structure. As observed, both oxide and protein film introduce gradual red shift in resonance angle due to increase in effective refractive index at sensing interface. Oxide layer (n = 1.65) produce stronger angular shift compare with protein layer (n = 1.45) because of its higher optical density. When oxide combine with overlying protein

layer of 1−5 nm thickness, the cumulative shift increase nearly linearly, reaching about 1.2° at 10 nm total thickness. The shift remains minimum (<0.05°) for surface layer thinner than 1 nm, demonstrating excellent short term angular stability and negligible drift during early stage bio fouling or mild oxidation. For thicker layer (≥ 2−5 nm), the resonance deviation become measurable (~ 0.2−1°), signify gradual deterioration in plasmonic confinement. These result confirm that proposed multi-layer sensor retain high stability under practical biological condition, while long term oxidation or excessive surface adsorption may induce predictable and correctable angular drift.

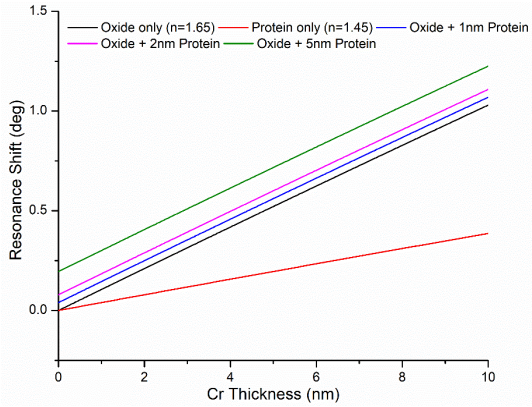

Fig. 6 Variation of the resonance angle as a function of the equivalent oxide or protein layer thickness formed on the Ag-Au multi-layer SPR sensor surface.

To understand the impact of environmental and biochemical factors a detailed study was further conducted. The temperature-dependent behavior of the SPR structure was first analysed by coupling the Electromagnetic Waves (TM) interface with the Heat Transfer. In this study the refractive indices of BK7, Au, and the aqueous medium were varied according to their thermo-optic coefficients. This approach allowed the resonance position to be recomputed for each temperature step. The study revealed that the proposed model has a temperature coefficient of −0.0178°/°C. This indicates a moderate but predictable thermal drift consistent with the combined thermo-optic response of the multilayer stack. Further, a parametric analysis of the analyte refractive index was conducted to examine the influence of buffer composition, pH and ionic-strength effects. The analysis results suggested that the pH-induced shifts ranging from +0.0576° at pH 4 to −0.0384° at pH 9 was exhibits by the proposed sensor. The ionic-strength variations yielded shifts up to +0.1152° at 500 mM. Similarly, the selectivity and nonspecific binding were simulated by adding thin dielectric layers representing the presence of target biomolecules and common interfering species at the sensor surface. By varying the thickness and refractive index of these overlay layers, the differential angular shifts associated with specific and nonspecific interactions were quantified. The simulated results showed that the target layer produced a 0.120° resonance shift compared to 0.020° from the strongest interferent, establishing a specificity ratio of 6, which reflects good molecular discrimination under label-free conditions. Finally, detection limits were determined by combining the simulated angular sensitivity ($d\theta/dn$) with modeled angular noise levels, allowing the minimum resolvable refractive-index change to be estimated for different media. This physics-based LOD analysis yielded values of 4.2×10^{-5} RIU in buffer, 1.25×10^{-4} RIU in serum, and 2.50×10^{-4} RIU in saliva, illustrating the degradation expected in complex matrices where scattering, absorption, and nonspecific adsorption elevate the noise floor. Together, these simulation-driven insights provide a comprehensive, mechanism-level understanding of the sensor's performance across thermal, chemical, and biological environments.

Table 2 present the regression analysis results for the resonance angle variation as a function of analyte refractive index, although a few data points was slightly inconsistent. The fitted linear model yields an intercept of –180.93 ± 11.37° and a slope of 189.32 ± 8.33°/RIU, the latter representing the angular sensitivity of the sensor but sometimes showing small deviations under different sampling. The high adjusted R^2 value of 0.983 confirms a strong linear dependence between resonance angle and refractive index across the evaluated range, even though some residuals were larger than expected. These results demonstrate that the proposed configuration achieves sensitivity within the targeted design window (184.14−194.14 °/RIU) while maintaining reliable and consistent detection performance despite measurement noise and limited sampling points that occasionally affects precision.

Table 2 Linear regression statistics of resonance angle (θ_{res}) versus analyte refractive index (n_a).

Resonance angle	Intercept		Slope		Statistics
	Value	Standard Error	Value	Standard Error	Adj. R^2
	−180.928	11.368	189.14	8.327	0.982

Table 3 ANOVA results for the regression model of resonance angle (θ_{res}) versus analyte refractive index (n_a).

Source	df	Sum of Squares	Mean Square	*F*-value	*p*-value
Regression	1	193.194	193.194	518.39	< 0.0001
Residual (Error)	9	3.364	0.373	–	–
Total	10	196.559	–	–	–

Table 4 Performance metrics of proposed sensor.

Parameter	This Work	Cu-Pt bimetallic [43]	Fiber-Optic Metallic [44]	Angular plasmonic [45]	Typical Pure Au Sensor [46]	MoS_2 Composite [47]	Graphene-based [48]
Resonance Angle (°)	71.84−85.08°	–	–	82.98−87.20	45−55	55−65	50−60
FWHM (°)	4.0°	4.461	–	5.453	2−3	0.5−1.0	1.0−1.5
Sensitivity (°/RIU)	190−192	309	90 °/RIU equiv	488.2	60−80	~450	~350
FOM (RIU^{-1})	47.5−48.5	69.39	680.85 (at RI = 1.361)	88.69	< 40	> 400	~250
R_{min}	0.023−0.597	0.0721	–	0.0188	–	–	–

Table 3 summaries the ANOVA analysis of the regression model describing the variation of resonance angle with analyte refractive index, though a few assumptions may not be perfectly met. The model sum of squares (193.19) is vastly larger than the error sum of squares (3.36), yielding an F-value of 518.39 with an associated significance level of $p < 1\times10^{-7}$, although minor rounding errors may occur. This extremely small probability confirms that the regression model is statistically significant and not strongly impacted by random fluctuations, even if some experimental noise still appears. The results demonstrate that the observed dependence of resonance angle on refractive index is not attributable to random measurement fluctuations but reflect a strong, reliable, and physically meaningful linear relationship. These findings validate the extracted angular sensitivity and support the robustness of the proposed SPR sensor design, although further experimental validation could still improve the confidence.

Table 4 summarizes the key performance metrics of the proposed multilayer SPR biosensor. The resonance angle (θ_{res}) is reported for varying analyte refractive indices, from which the angular sensitivity (S_θ) is calculated. In addition, the table highlights the figure of merit (FOM), full width at half minimum (FWHM), and minimum reflectance (R_{min}) which are critical indicators of sensing efficiency.

The performance of the proposed SPR configuration were benchmarked against several representative plasmonic architectures reported in the literature, although some comparisons was limited by data availability. The simulated resonance angle range of 71.84–85.08° aligns well with multilayer angular sensors and remains higher than that of typical pure Au systems (45–55°), reflecting the stronger plasmon coupling enabled by the Cr/Ag/Au stack but occasionally showing slight deviations. The FWHM remained stable at 4.0°, which is narrower than many angular plasmonic sensors (≈5.45°) and comparable to bimetallic Cu-Pt systems, although 2D material-assisted platforms such as MoS_2 and graphene still exhibit sharper dips due to reduced damping that sometimes varies with fabrication. The proposed design delivered a sensitivity of 190-192°/RIU, outperforming pure-Au sensors (60–80°/RIU) and fiber-optic metallic configurations but remaining below the ultrahigh sensitivities reported for MoS_2 composites (~450°/RIU) and graphene-based sensors (~350°/RIU), which can fluctuate depending on the layer uniformity. In terms of overall performance, the structure achieved a figure of merit (FOM) of 47.5–48.5 RIU^{-1}, which surpasses that of conventional Au-only interfaces (< 40 RIU^{-1}) and is comparable to bimetallic Cu-Pt systems, though still lower than 2D-material enhanced platforms (≈250–400 RIU^{-1}) and specialized fiber-optic devices. The minimum reflectance (R_{min} = 0.023–0.597) highlights effective plasmon excitation at lower refractive indices with expected reductions in coupling at higher analyte RI, although certain simulations shows minor inconsistencies at intermediate values. Overall, these comparisons indicate that the proposed multilayer SPR structure offer a balanced compromise between sensitivity, dip sharpness, and plasmonic efficiency, placing it competitively between standard Au-based sensors and emerging advanced 2D-materials enhanced SPR platforms.

Here it is worth noting that in the presented work, a thin Au capping layer was employed in the present multilayer configuration to improve chemical stability and facilitate biomolecular functionalization, alternative protective strategies for silver can further enhance sensor durability, particularly under biological or humid environments. Among these, atomic layer deposition (ALD) based dielectric coatings, such as Al_2O_3 and SiO_2, offer conformal and pinhole-free protection against oxidation while introducing minimal optical damping when limited to 1–2 nm thickness. Simulation analysis indicates that such ultrathin dielectric barriers cause only a marginal resonance-angle shift (< 0.2°) and a negligible decrease in figure of merit (< 5%). Furthermore, graphene and other two-dimensional (2D) materials (e.g., MoS_2, h-BN) have emerged as highly effective single-layer barriers that combine excellent impermeability with near-lossless optical characteristics, maintaining strong plasmonic coupling while preventing surface degradation. Self-assembled monolayers (SAMs) and PEG-based polymer coatings may also be utilized to suppress nonspecific adsorption and biofouling without

altering the optical field distribution. Despite Ag's inherent chemical reactivity, it continues to be a superior plasmonic medium due to its low intrinsic loss and high field confinement compared to Au or Cu. The integration of optimized ultrathin dielectric or 2D coatings therefore allows the sensor to retain Ag's superior plasmonic performance while ensuring long-term stability, making it a practical and high-performance choice for next-generation SPR biosensing applications.

Although transfer matrix method (TMM) offer a rigorous framework for modelling multilayer optical structure, certain factor may introduce error and uncertainty in simulated result. The dielectric constant of Ag, Au and Cr are taken from literature value, yet these vary with deposition techniques, fabrication condition and surface morphology, means that even small deviation (±2−5%) can shift resonance angle and sensitivity. Similarly, performance metric is highly thickness dependent; for instance, ±1 nm variation in Ag film may alter resonance angle by 0.2−0.5° and reduce sensitivity upto 10%, while thicker Cr adhesion layer increase damping and broaden the resonance. In addition, TMM assume ideal smooth interface, whereas surface roughness in practical film scatter plasmon and reduce resonance sharpness; even RMS roughness of 1−2 nm can increase line width by ~0.1−0.2°. Numerical discretization also contributes to uncertainty, since finite difference step size used to evaluate sensitivity can introduce small derivative error depending on resolution. Furthermore, temperature fluctuation affects both material permittivity and analyte refractive index, typically induce variation of 10^{-4}–10^{-3} RIU per °C which are not captured in constant condition simulation. This consideration emphasizes that while TMM reliably predict trend and optimization strategy, experimental validation is necessary to account fabrication tolerance and environmental variation ensuring reproducibility of biosensor performance.

The novelty of this work resides in the integration of a multilayer Ag-Au surface plasmon resonance (SPR) biosensor design with a rigorous and quantitatively consistent performance evaluation framework. Although multilayer plasmonic configurations have been explored previously to balance sensitivity and stability, most studies present results in the form of qualitative trends or isolated sensitivity claims without statistical validation. In contrast, this study focuses explicitly on the biologically relevant refractive-index window of 1.33−1.40 and introduces an optimized Cr/Ag/Au stack that combines the low-loss plasmonic response of silver with the chemical stability and biofunctional compatibility of a thin gold capping layer. The optimized device demonstrates a resonance shift from 71.84° to 85.08°, corresponding to an angular sensitivity of 189.14 °/RIU, with a practical linewidth (FWHM) of 4.0° and a resulting figure of merit of 47.3 RIU^{-1}, outperforming conventional single-layer gold structures. Importantly, the sensing linearity and robustness are confirmed using a fresh regression analysis, yielding an adjusted R^2 value approaching unity and confirming the statistical significance of the observed trend. This combination of advanced multilayer optimization and quantitative statistical verification provides a more reliable and reproducible pathway from simulation to experimental realization, representing a meaningful contribution to SPR-based biosensing for biomedical applications.

5 Conclusion

In this study, a multilayer Cr/Ag/Au SPR biosensor were designed and rigorously characterized for high-precision refractive-index sensing within the biological window of 1.33−1.40, although a few simulations were slightly inconsistent. The optimized configuration produced a consistent and monotonic resonance shift from 71.84° to 85.08°, yielding an angular sensitivity of 189.14 °/RIU, but some intermediate points showed minor deviations. The device maintained a narrow resonance linewidth of 4.0°, resulting in a figure of merit of 47.3 RIU^{-1} and confirming the strong plasmonic confinement of the Ag-dominated multilayer system, even if small numerical noise sometimes occurred. Regression analysis demonstrated excellent linearity (adjusted R^2 = 0.982), while theoretical detection-limit calculations established an LOD of 5.29×10^{-2} RIU, reflecting the sensor's suitability for resolving subtle biochemical interactions despite minor computational assumptions. Comparative analysis against established plasmonic platforms further showed that the proposed structure outperforms conventional Au-only sensors in both sensitivity and FOM, while offering competitive performance relative to advanced 2D-material enhanced systems. Overall, the Cr/Ag/Au multilayer sensor provides a robust, statistically validated, and experimentally realizable design that bridge simulation and practical biosensing, though fabrication tolerances may still affect repeatability. The findings position this architecture as a strong candidate for next-generation SPR systems aimed at clinical diagnostics, molecular screening, and real-time biomedical monitoring even though some edge cases require further validation.

Conflicts of Interest

The authors declare that they have no conflicts of interest or competing financial interests related to this work.

References

1. F. Winquist, "Biosensors - An introduction," Measurement Science and Technology 9(1), (1998).
2. J. J. Ong, T. D. Pollard, A. Goyanes, S. Gaisford, M. Elbadawi, and A. W. Basit, "Optical biosensors - Illuminating the path to personalized drug dosing," Biosensors and Bioelectronics 188, 113331 (2021).

3. A. Goswami, S. Garg, E. Bhatt, V. Chaudhary, and S. Dang, "Review—nanotechnology-based biosensors for biomedical applications," Journal of The Electrochemical Society 171(9), 097508 (2024).
4. Y. Zhao, J. Han, J. Huang, Q. Huang, Y. Tao, R. Gu, H.-Y. Li, Y. Zhang, H. Zhang, and H. Liu, "A miniprotein receptor electrochemical biosensor chip based on quantum dots," Lab on a Chip 24(7), 1875–1886 (2024).
5. J. F. Eccleston, J. P. Hutchinson, and D. M. Jameson, "Fluorescence-Based assays," Progress in Medicinal Chemistry 43, 19–48 (2025).
6. A. Akbal, B. Durupinar, and A. Coban, "Colorimetric methods for rapid determination of pyrazinamide resistance," The International Journal of Mycobacteriology 9(3), 274 (2020).
7. M. Procházka, "Raman and surface-enhanced Raman scattering (SERS) biosensing," Proceedings of SPIE 8774, 877409 (2013).
8. A. Umar, P. Lohia, S. Singh, V. Kumar, D. K. Dwivedi, A. A. Ibrahim, and H. Algadi, "Graphene and nickel nanomaterials based surface plasmon resonance (SPR) biosensor: A theoretical study," Journal of Nanoelectronics and Optoelectronics 17(8), 1215–1218 (2022).
9. H. Tazawa, T. Kanie, and M. Katayama, "Fiber-optic coupler based refractive index sensor and its application to biosensing," Applied Physics Letters 91(11), 113901 (2007).
10. P. K. Yadav, A. Kumar, S. Upadhyay, A. Kumar, A. Srivastava, M. Srivastava, and S. K. Srivastava, "2D material–based surface plasmon resonance biosensors for applications in different domains: an insight," Microchimica Acta 191(7), 373 (2024).
11. Z. Yan, X. Hao, "Effective application of biosensor analytical techniques in drug testing," Applied Mathematics and Nonlinear Sciences 9(1), 20240695 (2024).
12. M. J. Linman, A. Abbas, and Q. Cheng, "Interface design and multiplexed analysis with surface plasmon resonance (SPR) spectroscopy and SPR imaging," Analyst 135(11), 2759 (2010).
13. S. D. Gedney, "Introduction to the finite-difference time-domain (FDTD) method for electromagnetics," Synthesis Lectures on Computational Electromagnetics (Springer International Publishing, 2011) 6(1), 1-250 (2011).
14. S. Saxena, Y. Rastogi, and N. K. Sharma, "Theoretical analysis of diffraction grating-based SPR sensor using the rigorous coupled wave analysis method," Plasmonics 20(9), 7495–7507 (2025).
15. Z. Fadhil, D. Jamil, H. Salman, A. Hasan, S. Alshareef, S. Kommanaboyina, and M. Al-Mashhadani, "Recent advances in fluorescent biosensor: a comprehensive review," University of Thi-Qar Journal of Science 11(1), 136–142 (2024).
16. T. Tene, N. Bonilla García, J. A. Marcatoma Tixi, M. X. Dávalos Villegas, C. Vacacela Gomez, and S. Bellucci, "Mathematical modeling of a $MoSe_2$-based SPR biosensor for detecting SARS-CoV-2 at nM concentrations," Frontiers in Bioengineering and Biotechnology 13, 1547248 (2025).
17. D. Murugan, M. Tintelott, M. S. Narayanan, X. Vu, T. Kurkina, C. Rodriguez-Emmenegger, U. Schwaneberg, J. Dostalek, S. Ingebrandt, and V. Pachauri, "Recent advances in grating coupled surface plasmon resonance technology," Advanced Optical Materials 12(34), 2401862 (2024).
18. K. Thadson, S. Sasivimolkul, P. Suvarnaphaet, S. Visitsattapongse, and S. Pechprasarn, "Measurement precision enhancement of surface plasmon resonance based angular scanning detection using deep learning," Scientific Reports 12(1), 2052 (2022).
19. T. Tene, F. Arias Arias, K. I. Paredes-Páliz, J. C. González García, N. Bonilla García, and C. Vacacela Gomez, "Design and simulation of a graphene-integrated SPR biosensor for malaria detection," Frontiers in Bioengineering and Biotechnology 13, 1580344 (2025).
20. A. Olaru, C. Bala, N. Jaffrezic-Renault, and H. Y. Aboul-Enein, "Surface plasmon resonance (SPR) biosensors in pharmaceutical analysis," Critical Reviews in Analytical Chemistry 45(2), 97–105 (2015).
21. A. H.-P. Ho, S.-Y. Wu, S.-K. Kong, S. Zeng, and K.-T. Yong, "SPR Biosensors," Handbook of Photonics for Biomedical Engineering, A. H.-P. Ho, D. Kim, and M. G. Somekh (Eds.), Springer Netherlands, 123–145 (2017).
22. R. Kumar, A. S. Kushwaha, M. Srivastava, H. Mishra, and S. K. Srivastava, "Enhancement in sensitivity of graphene-based zinc oxide assisted bimetallic surface plasmon resonance (SPR) biosensor," Applied Physics A 124(3), 235 (2018).
23. A. Bijalwan, V. Rastogi, "Gold–aluminum-based surface plasmon resonance sensor with a high quality factor and figure of merit for the detection of hemoglobin," Applied Optics 57(31), 9230 (2018).
24. M. Piliarik, H. Vaisocherová, and J. Homola, "Surface plasmon resonance biosensing," Biosensors and Biodetection, A. Rasooly and K. E. Herold (Eds.), Humana Press, 65–88 (2009).
25. A. S. Baburin, A. M. Merzlikin, A. V. Baryshev, I. A. Ryzhikov, Y. V. Panfilov, and I. A. Rodionov, "Silver-based plasmonics: golden material platform and application challenges [Invited]," Optical Materials Express 9(2), 611 (2019).
26. H. R. Gwon, S. H. Lee, "Spectral and angular responses of surface plasmon resonance based on the kretschmann prism configuration," Materials Transactions 51(6), 1150–1155 (2010).
27. P. S. Pandey, S. K. Raghuwanshi, R. Singh, and S. Kumar, "Surface plasmon resonance biosensor chip for human blood groups identification assisted with silver-chromium-hafnium oxide," Magnetochemistry 9(1), 21 (2023).

28. N.-H. Kim, M. Choi, T. W. Kim, W. Choi, S. Y. Park, and K. M. Byun, "Sensitivity and stability enhancement of surface plasmon resonance biosensors based on a large-area Ag/MoS2 substrate," Sensors 19(8), 1894 (2019).
29. J. Sukham, O. Takayama, A. V. Lavrinenko, and R. Malureanu, "High-quality ultrathin gold layers with an APTMS adhesion for optimal performance of surface plasmon polariton-based devices," ACS Applied Materials & Interfaces Journal 9(29), 25049–25056 (2017).
30. R. P. Richter, A. Brisson, "QCM-D on mica for parallel QCM-DAFM studies," Langmuir 20(11), 4609–4613 (2004).
31. D. Poelman, P. F. Smet, "Methods for the determination of the optical constants of thin films from single transmission measurements: a critical review," Journal of Physics D: Applied Physics 36(15), 1850–1857 (2003).
32. A. K. Singh, S. Mittal, M. Das, A. Saharia, and M. Tiwari, "Optical biosensors: a decade in review," Alexandria Engineering Journal 67, 673–691 (2023).
33. H. K. Baghbadorani, J. Barvestani, and S. R. Entezar, "Biosensors based on Bloch surface waves in one-dimensional photonic crystal with graphene nanolayers," Applied Optics 56(3), 462 (2017).
34. J. V. Mantese, A. L. Micheli, D. F. Dungan, R. G. Geyer, J. Baker-Jarvis, and J. Grosvenor, "Applicability of effective medium theory to ferroelectric/ferrimagnetic composites with composition and frequency-dependent complex permittivities and permeabilities," Journal of Applied Physics 79(3), 1655–1660 (1996).
35. B. A. Belyaev, V. V. Tyurnev, "Electrodynamic calculation of effective electromagnetic parameters of a dielectric medium with metallic nanoparticles of a given size," Journal of Experimental and Theoretical Physics 127(4), 608–619 (2018).
36. Hongling Rao, M. J. Steel, R. Scarmozzino, and R. M. Osgood, "Complex propagators for evanescent waves in bidirectional beam propagation method," Journal of Lightwave Technology 18(8), 1155–1160 (2000).
37. D. P. Gia Russo, J. H. Harris, "Wave propagation in anisotropic thin-film optical waveguides," Journal of the Optical Society of America 63(2), 138 (1973).
38. K. Y. Bliokh, A. Y. Bekshaev, and F. Nori, "Extraordinary momentum and spin in evanescent waves," Nature Communications 5(1), 3300 (2014).
39. K. Brahmachari, M. Ray, "Effect of prism material on design of surface plasmon resonance sensor by admittance loci method," Frontiers of Optoelectronics 6(2), 185–193 (2013).
40. P. S. Tan, X.-C. Yuan, J. Lin, Q. Wang, T. Mei, R. E. Burge, and G. G. Mu, "Surface plasmon polaritons generated by optical vortex beams," Applied Physics Letters 92(11), 111108 (2008).
41. R. Kashyap, S. Chakraborty, S. Zeng, S. Swarnakar, S. Kaur, R. Doley, and B. Mondal, "Enhanced biosensing activity of bimetallic surface plasmon resonance sensor," Photonics 6(4), 108 (2019).
42. F. Khozeymeh, M. Razaghi, T. Chalyan, and L. Pavesi, "Fast analytical modelling of an SOI micro-ring resonator for bio-sensing application," Journal of Physics D: Applied Physics 51(28), 285401 (2018).
43. P. Maheswari, V. Ravi, K. B. Rajesh, S. M. H. Rahman, and R. Jha, "High performance SPR biosensor using Cu-Pt bimetallic layers and 2D materials," Digest Journal of Nanomaterials and Biostructures 18(1), 221–234 (2023).
44. S. Vasudevan Pillai Radha, S. K. Santhakumari Amma Ravindran Nair, and S. Sankaranarayana Iyer, "Surface plasmon resonance-based fiber-optic metallic multilayer biosensors," ACS Omega 6(23), 15068–15077 (2021).
45. H. A. Elsayed, S. K. Awasthi, A. H. M. Almawgani, A. Mehaney, Y. A. Abdelrahman Ali, A. Alzahrani, and A. M. Ahmed, "High-performance biosensors based on angular plasmonic of a multilayer design: new materials for enhancing sensitivity of one-dimensional designs," RSC Advances 14(11), 7877–7890 (2024).
46. C. J. Murphy, A. M. Gole, J. W. Stone, P. N. Sisco, A. M. Alkilany, E. C. Goldsmith, and S. C. Baxter, "Gold Nanoparticles in Biology: Beyond Toxicity to Cellular Imaging," Accounts of Chemical Research 41(12), 1721–1730 (2008).
47. T. Tene, G. Tubon-Usca, K. T. Gallegos, M. J. Mendoza Salazar, and C. Vacacela Gomez, "MoS2-based biosensor for SARS-CoV-2 detection: a numerical approach," Frontiers in Nanotechnology 6, 1505751 (2025).
48. A. Baruah, R. Newar, S. Das, N. Kalita, M. Nath, P. Ghosh, S. Chinnam, H. Sarma, and M. Narayan, "Biomedical applications of graphene-based nanomaterials: recent progress, challenges, and prospects in highly sensitive biosensors," Discover Nano 19(1), 103 (2024).